https://doi.org/10.2352/ISSN.2169-4451.2017.32.360

Elastomer Fatigue in Belt Fusing

David Battat; Lexmark, Int.; Lexington, Kentucky/United States of America

Abstract

*Fatigue failure often shows up towards the end of life in the backup roll (BUR) in belt fusing, as shown in **Figure 1**.*

This paper has two objectives: (1) To develop a model or description of what drives fatigue in an elastomer from material and loading perspectives, that can be applied in fusing irrespective of the particular application at hand; and (2) to use this capability to examine fatigue, clarify the reason for the catastrophic failure in printers, and identify directions to meet the spec on life, as well as assess the impact this might have on other fusing attributes.

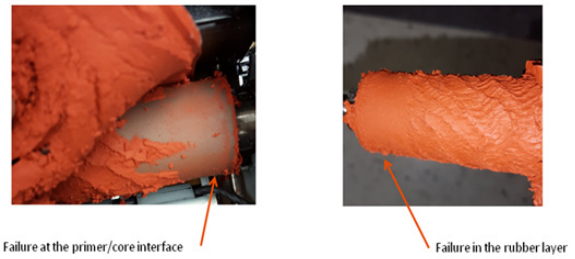

Figure 1. BUR Failures in the Rubber Layer or Primer / Core Interface at the End of the Roll

Synopsis

Two types of failures may be identified: delamination of the rubber at the core; and fatigue within the rubber. Evidence of delamination is seen by the presence of shiny metal core or the clean separation between rubber and core, indicating poor primer adhesion. The second failure mode, fatigue, is evidenced by crack propagation through the rubber and ultimate wholesale catastrophic break. Of note are the patterns of initiation of rubber failure both in the vicinity of the end of the roll, as well as at the metal core. The highly stressed interface at the core will fail where the material toughness is the lowest; if primer adhesion is up to spec then failure will occur within the rubber; on the other hand if primer adhesion is poor then de-lamination will be the failure mode.

Problems related to the primer are connected to manufacturing issues, often beyond direct control. To address fatigue, a model or criterion is required in order to understand what drives the process and what parameters are at our disposal. Gent's fatigue model in elastomers, which is based on Griffith's crack propagation theory, will be used to analyze the problem. This paper builds on Gent's approach and expands on it by introducing the concept of toughness to represent material properties. What emerges is a model which shows fatigue depends on two fundamental facets: material toughness at temperature, and the operating peak strain energy in the rubber; in other words what the material can sustain versus the actual loading applied.

The peak strain energy in the rubber does not depend on where stress or strain are highest in the system, rather it depends on where the total strain energy is maximum in the system, as represented by the strain components ε_y, ε_z, γ_{yz}. The peak strain energy occurs below the center of the nip, around 30-40% below the surface, at low loading. At high loading, the peak strain energy shifts to the rubber-core interface. As a point traverses the nip, it will experience a cycle of the strain energy, which promotes crack propagation in the material. In roll fusing, where the heater is inside the core tube, the rubber at the core experiences both high strain energy and high temperature, leading to low toughness and higher propensity to failure. In belt fusing, the core is not heated and the steady-state temperature of the BUR is not as high. Consequently, toughness at the core is not degraded, and failure is less likely. On the other hand, more and more is demanded from belt fusing in terms of features and low cost components, that there is a need to understand the mechanism and identify directions to obtain longer life.

The essence of fatigue analysis depends on knowing the actual load distribution along the roll. As the load varies with distance, so varies the peak strain energy. Axial load variations depend on a number of things: bending of the frame of the belt and BUR core; surface profiling of the backup roll; the profile of the core which affects rubber thickness along the axis; and the temperature distribution along the roll, which leads to thermal expansion of the rubber.

The question also arises as to what other fusing properties, such as paper handling, are affected once fatigue performance is improved.

Gent's Model for Fatigue in Elastomers

Rubber can fail by the action of cyclical loading even though the breaking stress is not exceeded. Gent's derivation [1] considers the test piece in **Figure 2**. The effect of the cut is to reduce the stored elastic energy, **W**, which is approximately $\mathbf{kC^2tW}$ where **k** is between **2** and $\boldsymbol{\pi}$. Thus, the rate of change in stored elastic energy per increment increase in cut is

$$-\frac{dW}{dc} = 2kCtW \qquad (1)$$

The **tear criterion** may then be expressed as

$$2kCW \geq T_E \qquad (2)$$

$\mathbf{T_E}$ is the tear energy. Equation 2 states that the tear will grow when the applied elastic energy equals or exceeds the tear strength of the material.

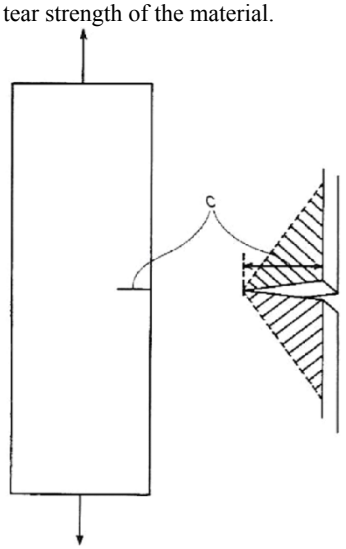

Figure 2. Tear Test Piece

The growth step **ΔC** per stress application and the tear energy $\mathbf{T_E}$ may be related

$$\Delta C = B T_E^a \tag{3}$$

B is cut growth constant and **a** (between 2 and 4) is the slope of the logΔC-logT_E curve. By using Equation 3 to substitute for $\mathbf{T_E}$ in Equation 2, the growth law per cycle of the crack may be written as

$$\frac{\Delta C}{C^a} = (2kW)^a B \Delta n \tag{3}$$

The length of the crack after **n** cycles is obtained by integration and the following expression results:

$$\frac{1}{C_o^{a-1}} - \frac{1}{C_f^{a-1}} = (a-1)[(2kW)^a B]n$$

where $\mathbf{C_o}$ is the initial and $\mathbf{C_f}$ is the final length of the crack. If $\underline{\mathbf{C_f}} \gg \underline{\mathbf{C_o}}$, the fatigue life **N**, i.e. the number of deformation cycles required to bring about rupture, is given by

$$N = \left[(a-1)(2kW)^a B C_0^{a-1}\right]^{-1} \tag{4}$$

Here **W=SE** is the input strain energy (**SE**) per cycle, and **k** is a constant approximately equal to 2. For natural rubber **a=2**; for elastomeric materials that do not exhibit crystallization on straining, **a≈4**.

Gent's formalism is extended by postulating in Equation 4 that when N=1, i.e. material fails in one cycle, the strain energy assumes its upper value and is equal to the material toughness or break value, $(SE)_{max}=W_b$. Then, solving for **B** one obtains

$$B = \left[(a-1)(2kW_b)^a C_0^{a-1}\right]^{-1} \tag{5}$$

This shows that **B** and $\mathbf{W_b}$ are inversely proportional. **B** is a measure of how much a cut or flaw within an elastomer sample will grow per cycle when subjected to a given tear energy. $\mathbf{W_b}$ is a measure of how much energy per unit volume is required to fracture an elastomer sample in one stress/strain cycle. Using Equation 5 to substitute for **B** in Equation 4, one obtains the number of cycles to failure as

$$N = \left(\frac{W_b}{SE}\right)^a \tag{6}$$

Equation 6 indicates that the number of cycles to failure **N** depends on the ratio of breaking energy $\mathbf{W_b}$ to applied strain energy **SE**, all raised to power '**a**'. Index **a** is determined experimentally by gradually increasing the input $\mathbf{T_E}$ in the specimen and observing the growth **ΔC.**

Energy-to-break

Toughness may be represented as an Arrhenius relationship. Thus, the equation for the energy-to-break as a function of temperature may be written as

$$W_b = W_{bo}\ Exp\left[\frac{E_a}{R}\left(\frac{1}{T} - \frac{1}{T_o}\right)\right] \tag{7}$$

If tensile strength at ambient temperature is σ = 2.2 MPa and elongation ε = 220% then energy-to-break is W_{bo} = σε/2 =350 psi @ Room Temperature. The activation energy E_a may be obtained from measurements of σ and ε at various temperatures, and from the slope of the log-log curve. Taking as example E_a=1722 cal/mole, Equation 7 becomes fully determinate.

The effect of temperature on energy-to-break can be examined by using Equation 7. Raising the temperature from 100°C to 200°C reduces toughness from 196 lb-in/in^3; to 120 lb-in/in^3, whereas at RT it is 351 lb-in/in^3. The effect on number of cycles to failure **N** can be inspected using Equation 6 while keeping strain energy constant. The ratio of cycles at RT to cycles at temperature, for a crack propagation constant **a=3**, shows a dramatic drop. Thus, increasing BUR temperature from RT to 100 and 200°C reduces cycles to failure by a factor of 5.8, and 25.3, respectively.

Strain Energy

Derivation

In plane strain, the following strain components are zero, and u, v, w the deformations along x, y, z respectively

$$\gamma_{xy} = \frac{\partial u}{\partial y} + \frac{\partial \mathrm{v}}{\partial x} = 0$$

$$\gamma_{zx} = \frac{\partial w}{\partial x} + \frac{\partial \mathrm{u}}{\partial z} = 0$$

$$\varepsilon_x = 0$$

Here, the x-axis is parallel to the BUR axis, the y-axis is inwards from the center of the nip along the radius, and the z-axis is tangential to a cross-section of the roll. The strain energy per unit volume, V_0, is given by Timoshenko and Goodier [2]:

$$V_o = \frac{1}{2}\lambda\left(\varepsilon_x + \varepsilon_y + \varepsilon_z\right)^2 + G(\varepsilon_x^2 + \varepsilon_y^2 + \varepsilon_z^2) + \\ + \frac{1}{2}G(\gamma_{xy}^2 + \gamma_{yz}^2 + \gamma_{zx}^2)$$

which reduces for the plane strain case to

$$V_o = \frac{1}{2}\lambda\left(\varepsilon_y + \varepsilon_z\right)^2 + G(\varepsilon_y^2 + \varepsilon_z^2) + \frac{1}{2}G\gamma_{yz}^2$$

Upon setting $\lambda = E_1\nu/(1+\nu)(1-2\nu)$ and $G = E_1/2(1+\nu)$ where $\mathbf{E_1}$ is the modulus of the upper layer, **G** is the modulus of elasticity in shear, and **ν** is Poisson's ratio, one obtains the following:

$$V_o = \frac{E_1(1-\nu)}{2(1+\nu)(1-2\nu)}\left[\varepsilon_y^2 + \varepsilon_z^2 + \frac{2\nu}{1-\nu}\varepsilon_y\varepsilon_z\right] + \frac{E_1}{4(1+\nu)}\gamma_{yz}^2$$

The value **ν=1/2** leads to $\boldsymbol{\varepsilon_y = -\varepsilon_z}$. Hence the last equation reduces to

$$V_o = \frac{2E_1}{3}\left[\varepsilon_z^2 + \frac{1}{4}\gamma_{yz}^2\right] \tag{8}$$

Equation 8 is the strain energy at any point in the rubber. It has two components, one due to a compressive strain $\boldsymbol{\varepsilon_z}$ and a second component due to shear strain $\boldsymbol{\gamma_{yz}}$. On the top surface, the shear is zero by definition and strain energy depends on $\boldsymbol{\varepsilon_z}$ only. For a soft on hard, e.g. rubber on steel, along the interface at the core, compressive strain is zero and strain energy depends on shear strain $\boldsymbol{\gamma_{yz}}$ alone.

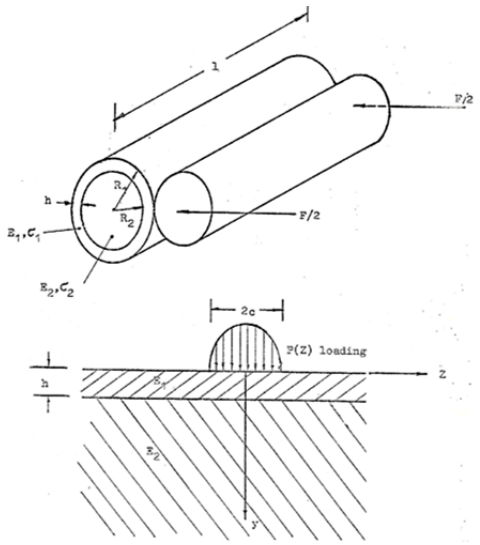

Figure 3. Contact problem of a layered cylinder loaded against solid roller (top); mathematical model – two-layer half space subjected to elliptical loading over a strip (bottom)

Solving the Biharmonic Equation of elasticity for a two layer structure with an elliptical load distribution as shown in **Figure 3**, a dimensionless form of the strain energy in the upper layer is obtains as

$$\left(\frac{R}{h}\right)^2\left(\frac{V_o}{E_1}\right)=\frac{2}{3}\left(\frac{\xi}{t}\right)^2\left[I_1^2+I_2^2\right] \qquad (9)$$

where

$$I_1=\int_0^\infty \Omega_1(\beta,y')J_1(\beta t)\cos(\beta tz')d\beta$$

$$I_2=\int_0^\infty \Omega_2(\beta,y')J_1(\beta t)\sin(\beta tz')d\beta$$

$$z'=z/c;\ y'=y/h$$

$$\Omega_1(\beta,y')=\frac{M^2y'e^{-y'\beta}+2M\{y'\sinh y'\beta-2\beta(1-y')\cosh y'\beta\}e^{-2\beta}-y'e^{(y'-4)\beta}}{M^2-2M\left(1+2\beta^2\right)e^{-2\beta}+e^{-4\beta}}$$

$$\Omega_2(\beta,y')=\frac{M^2y'e^{-y'\beta}+2M\{2\beta(1-y')\sinh y'\beta-y'\cosh y'\beta\}e^{-2\beta}+y'e^{(y'-4)\beta}}{M^2-2M\left(1+2\beta^2\right)e^{-2\beta}+e^{-4\beta}}$$

$$M=\frac{E_1/E_2+1}{E_1/E_2-1}\ ;\xi(t)=\frac{4}{\pi}\frac{F}{l}\frac{R\left(1-\nu^2\right)}{E_1h^2}$$

To compute the strain energy at point **y,z**, the variable **t**, which is half the nip to thickness ratio, is specified together with moduli ratio $\mathbf{E_1/E_2}$. The load function **ξ(t)** depends on **t** (as obtained from an algorithm), as shown in **Figure 4**.

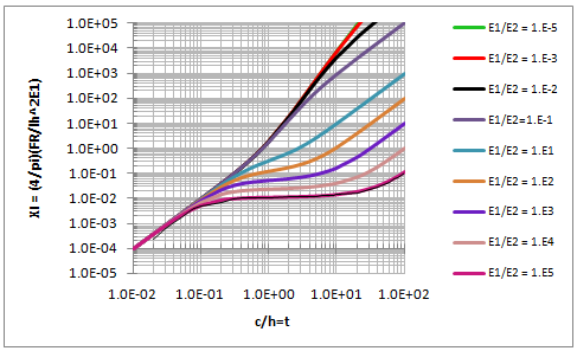

Figure 4. Relationship between nip width and load function

Contour Plots

The strain energy is calculated from Equation 9. In order to locate where the peak strain energy is within the rubber, contours of constant value of the energy in the domain of the upper layer at different loading conditions, are generated. Figures 5-7 depict the strain energy contours for the soft on hard system. Since the behavior is symmetric, only one half of the nip is shown, but with full depth of the thickness. **y′=0** represents the top surface, and **y′=1** represents the interface between rubber and core. Each figure is given for a specific value of **t**. The contours represent constant values of the dimensionless quantity $(R/h)^2(V_o/E_1)$.

The salient feature of the plots is that there is a location or region where strain energy is highest. For **t<1**, the compressive part of the strain energy tends to dominate and the maximum strain energy occurs at the center of the nip, about two thirds of the way up from the core. However, for **t ≥ 1** the shear component of the strain energy dominates and the maximum strain energy moves to the core in the vicinity of nip entrance / exit. As an example, for **t=1.5**, he peak strain energy is between **z′=0.75** and **z′=1**; the value for peak strain energy is $(R/h)^2(V_o)_{\max}/E_1=0.93$.

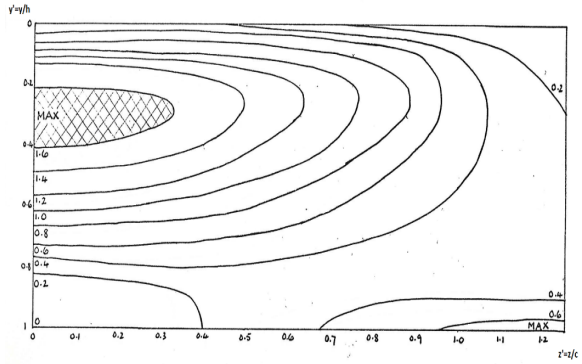

Figure 5. Contours for t = 0.5. y'=y/h; z'=z/c

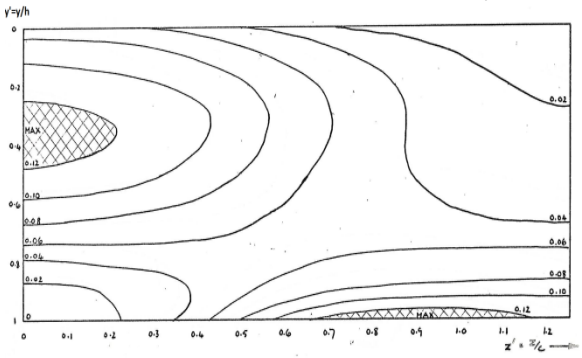

Figure 6. Contours for t = 1.0. y'=y/h; z'=z/c

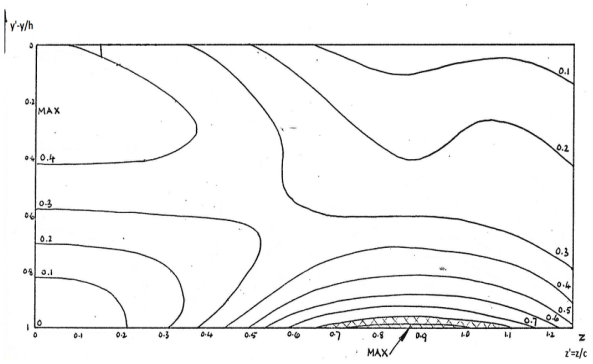

Figure 7 - Contours for t = 1.5. y'=y/h; z'=z/c

Regression for Peak Strain Energy

Regression of peak strain energy is shown in **Figure 8**. SEY represents the peak strain energy along **y** axis, and SEZ represents the peak strain energy along the rubber core interface. The intersection of the two curves occurs close to **t=0.975**.

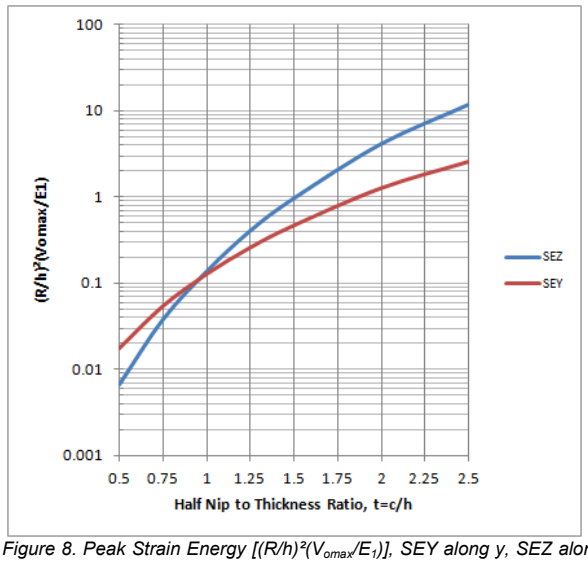

Figure 8. Peak Strain Energy [(R/h)²(V$_{omax}$/E$_1$)], SEY along y, SEZ along z

In belt fusing applications, the peak is at the rubber-core interface. A regression of the curve SEZ yields the expression

$$SE_{\max} = 0.15\frac{h^2}{R^2} E\, t^{4.75} \qquad (11)$$

By combining this expression with the regression between the load function **ξ** and **t** ($t = 0.7871\,\xi^{0.316}$), and using the definition of **ξ** given above, the peak strain energy may be expressed more explicitly as

$$SE_{\max} = 0.0483\frac{(N/l)^{1.583}}{E^{0.583}\, h^{1.167}\, R^{0.417}} \qquad (12)$$

Equation 12 is valid for $t \le 2.5$ and soft-on-hard. The strongest dependence is on load, followed by rubber thickness; the effects of rubber modulus and roll radius are the weakest.

Beams on Flexible Foundations

The above results are true only at a given cross section along the roll. In practice the load changes axially, being usually higher at the ends than in the middle. A method based on Beams on Elastic Foundations by Hetenyi [3] may be used to determine axial load variation, as shown in **Figure 9**. The deformation along the roll due to bending and due to surface profiling obtains as Equation 13.

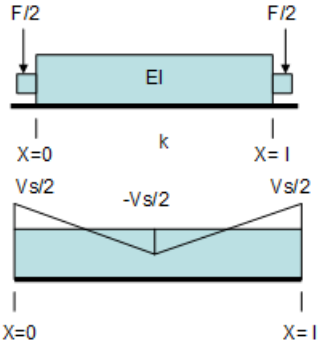

Figure 9. Beam on Elastic Foundation, k Spring Constant

$$y(x) = \frac{F}{l}\frac{l^4}{4EI}\frac{1}{A^3}\frac{\cosh(Ax/l)\cos(Ax/l') + \cosh(Ax/l')\cos(Ax/l)}{\sinh(A)+\sin(A)} + \mathrm{v}_S\left(1/2 - 2x/l\right);\quad 0 \le x \le l/2 \qquad (13)$$

EI is the combined rigidity of the belt frame and the core of the BUR; $\mathbf{v_s}$ is the maximum saddle of a parabolic surface profile on the BUR, $\mathbf{l' = l - x}$, and **A** is material wavelength given by

$$A^4 = \frac{1}{\mathrm{v}}\frac{F}{l}\frac{l^4}{4EI} \qquad (14)$$

In Equation 14, **v** is the **2D** indentation of the rubber, which occurs when the flexure and contact problems are combined. The load distribution **f(x)** obtains from the deformation profile **y(x)** as given next:

$$f(x) = k\,y(x) = \frac{1}{\mathrm{v}}\frac{F}{l}y(x) \qquad (15)$$

Rigidity **EI** may be determined from calculations or from nip measurements by matching experimental nip flare with the modulus that would reproduce the measured nip distribution, **Figure 10**.

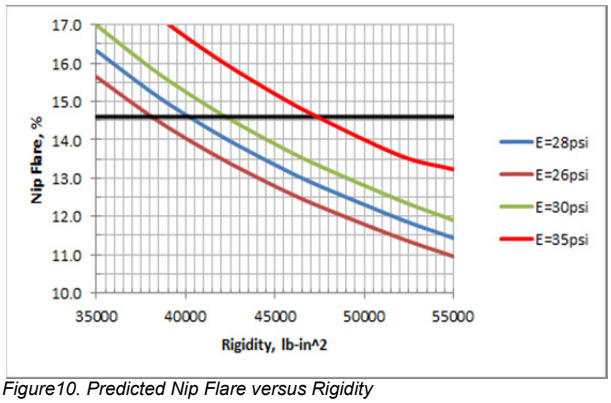

Figure10. Predicted Nip Flare versus Rigidity

Fatigue Life Prediction

Model elements:

1. A fatigue model
2. Energy to break at temperature
3. Peak strain energy and location in the nip
4. Load variation due to bending and profiling

Figure shows the load variation along roll axis for three different conditions: high load with large roll; medium load with medium roll; and medium load with small roll.

Figure 12 shows the peak strain energy variation for the three cases, which occurs at the rubber core interface.

Figure 13 shows the fatigue life in Kprints along the roll. Observations: life at edges is much shorter than in the middle, hence onset of failure is expected to be at the edges, at the core.

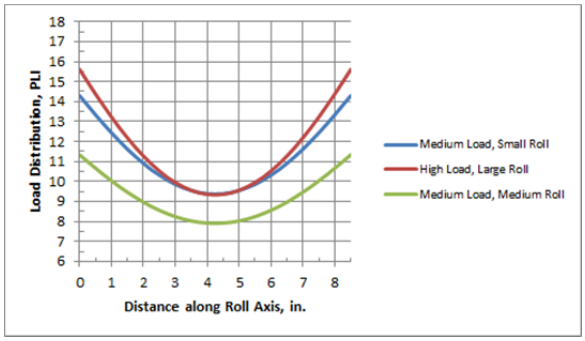

Figure 11. Comparison of Load Distribution along Roll Axis

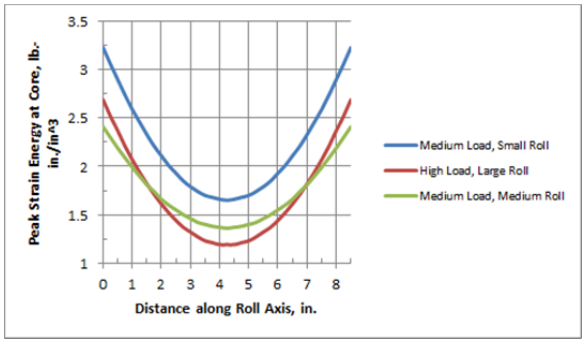

Figure 12 - Comparison of Strain Energy Distribution along Roll Axis

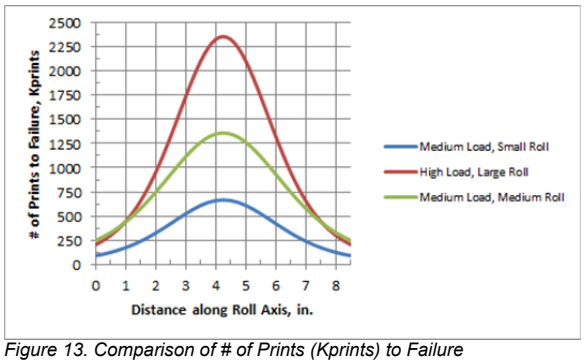

Figure 13. Comparison of # of Prints (Kprints) to Failure

Thus, bending, and to a lesser extent surface profiling, lead to a large drop in fatigue life from the center of the roll to the edges. Stressful conditions due to factors such as high load and small radius could cause the fatigue life at the edges to be close or below spec, leading to premature failures.

Life Improvement

This depends on two main variables, energy-to-break, and peak strain energy in the rubber. Relative to strain energy, Equation12 indicates that peak strain energy at the core depends strongly on load to the power 1.583. Rubber modulus, rubber thickness, and roll radius, offer opportunities to reduce strain energy but to a lesser extent.

Figure 14 shows the effect of load reduction on fatigue life, with emphasis at the edges of the roll. Nominal load (Blue), 10% reduction (Red), 16% reduction (green) curves indicate an improvement in life at the edges by a factor of about 2.5. While load reduction improves life, it could have an adverse effect on image fix paper handling.

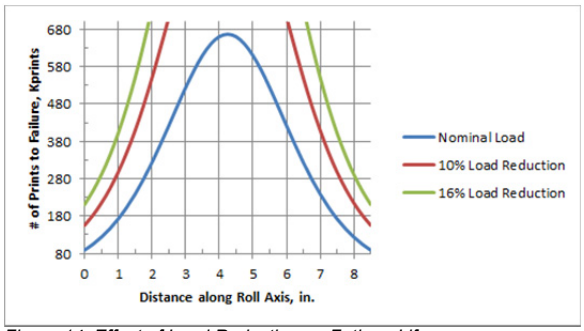

Figure 14. Effect of Load Reduction on Fatigue Life

Increased Rubber Toughness

A second approach for improvement of fatigue life is to increase the energy-to-break. Increasing rubber toughness is often more effective than reducing load. **Figure 15** illustrates what happens as filler content is increased. Toughness initially increases then falls. At low filler content, strain is high but stress is low, while at high filler content, strain is low but stress is high. At some intermediate point the highest energy to break is obtained.

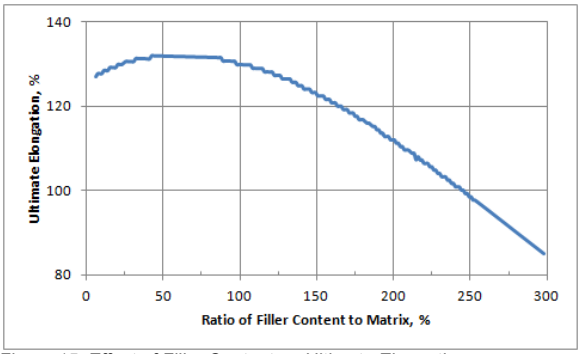

Figure 15. Effect of Filler Content on Ultimate Elongation

The Larger Picture

Ideally, life improvement should be considered from a system's perspective since any change one makes can affect other attributes of the system. One approach is to consider load; and rubber modulus as main driving factors:

Load and rubber modulus affect fatigue life through strain energy and energy to break.

Image fix is also affected by load and modulus as these two variables determine belt temperature required to fuse the image with a specific toner.

Paper handling, specifically paper wrinkle is affected by paper feed rates along the axis. These in turn are affected by load and modulus through nip flare.

Concluding Remarks

Two types of failure may be apparent in BUR, de-lamination of the rubber at the core, and fatigue within the rubber. Delamination is seen by the presence of the shiny metal core or clean separation at the core, indicating poor primer adhesion. Fatigue, is evidenced by propagation of crack through the rubber and ultimate break. Of note are the patterns of initiation of rubber failure both at roll end and at the core. The highly stressed interface at the core will fail where the material toughness is the lowest, either due to poor primer adhesion or high temperature.

Two main issues are addressed (1) understanding what fatigue in an elastomer involves, and in particular the duality between the energy to break or toughness of the rubber; and (2) the applied strain energy. The energy to break is represented by an Arrhenius relationship to be supplemented by the activation energy from testing or supplier's data. Relative to strain energy, the magnitude and location of the peak value in the system is determined by solving the Biharmonic Equation of elasticity. It is found that the peak value at low loading occurs below the nip center, about one third down the thickness; at high loading, the location moves to the rubber - core interface. Under fusing conditions, the latter situation prevails. A key aspect of the analysis is the determination of load distribution along roll axis and the integration of the flexure problem with the contact problem.

Computations show that due to bending of the system, there is a large drop in fatigue life from center to edge. The ends, especially at the core, have a much higher likelihood of failure than the center. Directions for improvement are identified, such as reducing load, and increasing rubber toughness

References

[1] "Fracture, An Advanced Treatise", edited by H. Liebowitz, Vol. VII, Chapter 6, A.N. Gent, 'Fracture of Elastomers' , p335. Academic Press 1972

[2] "Theory of Elasticity", S. Timoshenko and J.N. Goodier, p148, eq 85, McGraw-Hill Book Company 1951

[3] Hetenyi, "Beams on Elastic Foundations", Ann Arbor, 1964.

Author Biography

David Battat received his DPhil in Engineering Science from Oxford University. England. He was Principal Scientist with Xerox Corporation in Webster, NY. He has worked with Lexmark International in Lexington, KY since 2007.